Applied Catalysis B: Environmental 224 (2018) 46–52

Contents lists available at ScienceDirect

Applied Catalysis B: Environmental

journal homepage: www.elsevier.com/locate/apcatb

Research Paper

Charge-regulated sequential adsorption of anionic catalysts and cationic photosensitizers into metal-organic frameworks enhances photocatalytic proton reduction

He Li[a,1], Shuang Yao[b,1], Hong-Li Wu[a], Jing-Yan Qu[a], Zhi-Ming Zhang[a,b,*], Tong-Bu Lu[b], Wenbin Lin[c,*], En-Bo Wang[a]

[a] Key Laboratory of Polyoxometalate Science of Ministry of Education, Department of Chemistry, Northeast Normal University, Changchun, Jilin 130024, China
[b] Institute of New Energy Materials & Low Carbon Technology, Tianjin Key Laboratory of Organic Solar Cells and Photochemical Conversion, Tianjin University of Technology, No. 391 Binshuixi Road, Tianjin 300384, PR China
[c] Department of Chemistry, University of Chicago,929 East 57th Street, Chicago, IL 60637, United States

ARTICLE INFO

Keywords:
Polyoxometalate
Metal-organic framework
Composite materials
Hydrogen production

ABSTRACT

We have developed a simple, general, and efficient method for constructing photocatalytic active metal-organic framework (MOF)-based composite materials for visible light-driven hydrogen production. Here, several transition metal-substituted Wells – Dawson-type polyoxometalates (POMs) were successfully immobilized into a Cr-MOF of the MIL-101 structure, resulting in a series of POM@MOF composite materials [POM = $K_8HP_2W_{15}V_3O_{62}{\cdot}9H_2O$ ($P_2W_{15}V_3$), $K_8P_2W_{17}(NiOH_2)O_{61}{\cdot}17H_2O$ ($P_2W_{17}Ni$), $K_8P_2W_{17}(CoOH_2)O_{61}{\cdot}16H_2O$ ($P_2W_{17}Co$)]. We adjust the charge of MIL-101 framework by introducing Wells – Dawson-type POM anions with highly negative charge into the MOF. The MIL-101 framework absorbs the anionic POM, while the charge overcompensation in the POM@MOF composites allow them to efficiently adsorb cationic dyes. These composite materials accommodate and enrich cationic photosensitizer (PS) ruthenium(II) tris(bipyridyl) ($Ru(bpy)_3^{2+}$) from the solution, allowing the PSs to surround the POM proton reduction catalysts, resulting in a heterogeneous catalytic device POM@PSs@MOF with much higher photocatalytic activity than that of the corresponding homogeneous catalytic system. POM@MIL-101 could also be readily recycled and reused in catalytic reaction. Furthermore, this strategy was extended to sequential adsorption of anionic $Mo_2S_{12}^{2-}$ and cationic PSs to lead to highly active photocatalytic proton reduction system with a H_2 evolution rate of up to 25578 $\mu molh^{-1}g^{-1}$ (corresponding to $Mo_2S_{12}^{2-}$ catalyst) in 8 h under visible light irradiation.

1. Introduction

Commonly used as a source of energy, fossil fuels are not only nonrenewable but also produce harmful byproducts during combustion. In contrast, solar energy has the potential to provide a large scale, clean, and renewable energy source, causing widespread interest in developing efficient methods of converting sunlight energy into chemical energy [1–5]. Light-driven catalytic processes, including photocatalytic water splitting for hydrogen evolution, play a critical role in the conversion and storage of solar energy.

Polyoxometalates (POMs) have attracted considerable interest in many fields owing to their various structural characteristics, highly negative charges, and excellent redox ability [6–8]. Recently, they have been studied as photocatalysts for water splitting because they can undergo fast, reversible, stepwise multiple electron transfer reactions without alteration to their structures [9–12]. To date, only a few common POMs, such as $[P_2W_{18}O_{62}]^{6-}$ and $[H_2W_{12}O_{42}]^{10-}$, as well as Ta- and Nb-containing POMs have been explored as homogeneous hydrogen production catalysts. However, most of these studies rely on using either Pt(0) as a co-catalyst or require strong UV light irradiation [13–15]. Recently, with the aim of overcoming these limitations, transition metal-substituted POMs have also been studied as visible light-driven photocatalysts for water splitting [16–22].

Metal-organic frameworks (MOFs), a new class of molecular materials built from organic linkers and inorganic metal nodes, have attracted much attention over the past two decades. Their well-defined structures, high porosities, and tunable pore sizes and compositions make them potentially suitable for a diverse range of applications,

* Corresponding author.
E-mail addresses: zmzhang@email.tjut.edu.cn, zhangzz888@163.com (Z.-M. Zhang), wenbinlin@uchicago.edu (W. Lin).
[1] These authors contributed equally.

http://dx.doi.org/10.1016/j.apcatb.2017.10.031
Received 15 August 2017; Received in revised form 1 October 2017; Accepted 11 October 2017
Available online 12 October 2017

including gas separation and storage, catalysis, and drug delivery [23–28]. Traditionally, MOFs with specific active sites were either directly synthesized solvothermally (direct assembly) or covalently modified to produce specific sites after the synthesis of MOFs (post-synthetic functionalization). These two strategies provide complementary methods for constructing functional MOF materials [29–38]. Several functional UiO MOFs have been prepared via direct assembly, whereas a number of interesting MOF materials based on MIL-101 and ZIFs have been synthesized via postsynthetic functionalization [39–42]. Recently MOFs were shown to provide a highly tunable platform for the integration of antenna molecules and catalysts into efficient photocatalytic systems for solar energy harvesting [43–49]. In these studies, photosensitizing MOFs were constructed using photoactive organic or metal-organic ligands, such as porphyrin, $[Ru(bpy)_3]^{2+}$, and $[Ir(bpy)(py)_2]^{+}$-based chromophores, as the bridging linkers [50–57]. Although these studies provide an excellent method of constructing photosensitizing MOFs capable of proton reduction, CO_2 reduction, water oxidation, and photocatalytic oxidative degradation of organic molecules, they rely on the elaborate multi-step synthesis of complex photoactive linkers, which limits the applicability of this strategy to construct photocatalytic MOF materials based on many commonly used building blocks.

2. Experimental section

2.1. Materials and methods

All chemicals were commercially purchased and used without further purification. $K_8H[P_2W_{15}V_3O_{62}]\cdot 9H_2O$ [58], $K_8P_2W_{17}(NiOH_2)O_{61}\cdot 17H_2O$ [59], $K_8P_2W_{17}(CoOH_2)O_{61}\cdot 16H_2O$ [59], and $(NH_4)_2[Mo_2(S_2)_6]\cdot 2H_2O$[60] were synthesized according to the references. Elemental analyses of Cr, W, V, Co and Ni were performed with a Leaman inductively coupled plasma (ICP) spectrometer. TG analyses were performed on a DTG-60 AH instrument in flowing N_2 with a heating rate of 10 ° C min^{-1}. Powder X-ray diffraction (XRD) patterns were recorded with a D/max-IIIC diffractometer. IR spectra were recorded on an Alpha Centauri FT/IR spectrophotometer in the range 400–4000 cm^{-1}. UV–vis absorption spectra were recorded on a 756 CRT UV–vis spectrophotometer. Luminescence decays were taken with a 600 MHz LeCroy digital oscilloscope from an optical parametric oscillator. Steady-state photoluminescence spectra were tested by a SHIMADZU RF-5301PC spectrofluorometer.

2.2. Synthesis

A series of POM@MIL-101 composites were synthesized according to the following method. H_2bdc (terephthalic acid, 332 mg, 2 mmol) was added to 10 mL deionized water solution containing 86 mg tetramethylammonium hydroxide (TMAOH). The mixture was stirred at room temperature for 15 min, before adding $[Cr(NO_3)_3]\cdot 9H_2O$ (800 mg, 2 mmol), resulting in a dark blue colored suspension. Subsequently, a fixed amount of α-$PW_{15}V_3$ (80 mg, 160 mg, 200 mg, 240 mg, 400 mg, 600 mg and 800 mg) was added into this solution, which was stirred for another 20 min. The resulting mixture was added into a 20 mL Teflon lined autoclave and heated at 453 K for 72 h. After cooling slowly to ambient temperature, the green powder was collected and thoroughly washed with distilled water, hot DMF (50 °C) and methanol several times. The products were dried at room temperature, resulting in a 80% yield based on chromium ($PW_{15}V_3$@MIL-101). The synthesis of POM@MIL-101 composites with other two POMs was similar to that of $PW_{15}V_3$@MIL-101, by simple replacement of the α-$PW_{15}V_3$ with α-$P_2W_{17}Ni$ and α-$P_2W_{17}Co$ in the synthetic process. These POM@MIL-101 composites with different amounts of POMs ($P_2W_{15}V_3$, $P_2W_{17}Ni$ and $P_2W_{17}Co$) 80 mg, 160 mg, 200 mg, 240 mg, 400 mg, 600 mg, 800 mg, were named V-1 to V-7, Ni-1 to Ni-7, and Co-1 to Co-7, respectively.

2.3. Visible light-Driven hydrogen production

Photocatalytic H_2 production was carried out in an external illumination-type reaction vessel with constant stirring at room temperature. In a typical experiment, photocatalytic H_2 production was performed in a 16 mL DMF/CH_3CN (7/3) mixed solution containing 94 mM triethanolamine (TEOA), and 200 μL pH 2.0 water (adjusted by 2 M HCl). The POM@MOF composite **V-1** with 3.1 μM of $P_2W_{15}V_3$ catalyst and the PS $[Ru(bpy)_3]^{2+}$ (48 μM) were added into the solution. The vials were capped and deoxygenated by bubbling nitrogen through them for 20 min to ensure the air was completely removed. The solution was irradiated by a 300W Xe-light with a 420 nm filter. After the hydrogen evolution reaction, the gas in the headspace of the vial was analyzed by gas chromatography using a GC7900 instrument to determine the amount of hydrogen generated. Photocatalytic H_2 production of other composites $PW_{17}Ni$@MIL-101 and $PW_{17}Co$@MIL-101 was performed similar to that of $PW_{15}V_3$@MIL-101.

3. Results and discussion

The POM@MOF composite materials ($P_2W_{15}V_3$@MIL-101, $P_2W_{17}Ni$@MIL-101, and $P_2W_{17}Co$@MIL-101) were synthesized through a one-pot reaction of POMs, Cr^{3+} ion, tetramethylammonium hydroxide (TMAH), and terephthalic acid (H_2bdc) (Scheme 1). ICP, TG, XRD, FTIR, and EDX analysis were performed to determine the structure and composition of the composites to confirm that the POMs were successfully encapsulated in the porous framework (Fig. 1, S1 to S3). As shown in Fig. 1a, the atomic ratio (W/Cr) increased by raising the loading amount of POMs. However, when the amount of POM reached or exceeded 600 mg, the loading amount of POM in the composite materials remained almost unchanged, suggesting that the limit was reached. According the ICP results, the formula of the composites $P_2W_{15}V_3$@MOFs were determined as POM@34MOFs, POM@14MOFs, POM@9MOFs, POM@8MOFs, POM@6MOFs, POM@5MOFs and

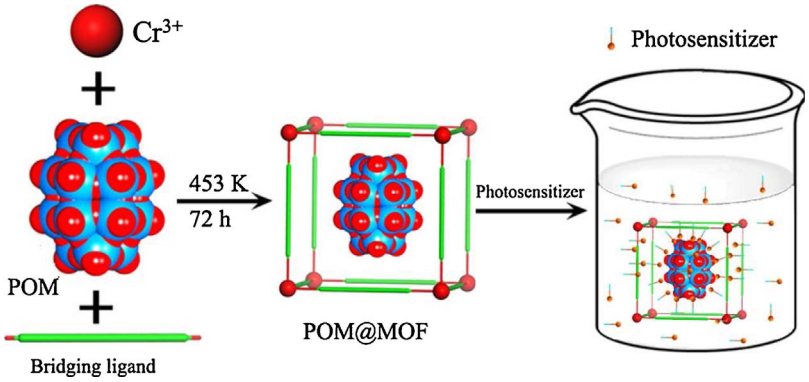

Scheme 1. Scheme view for constructing POM@MOF and POM@PSs@MOF composite materials.

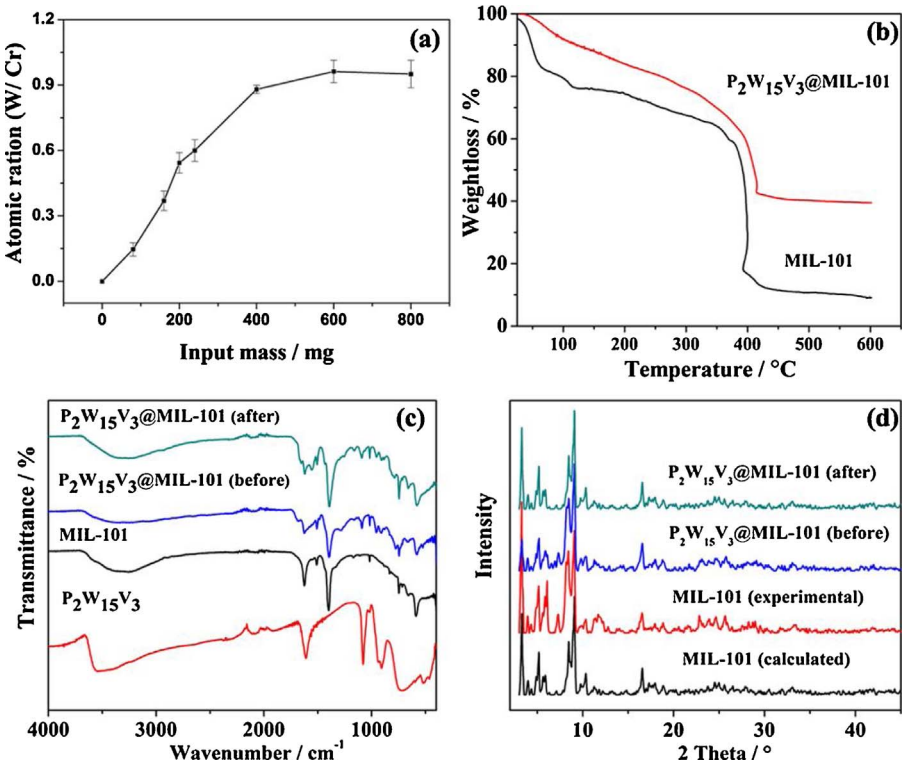

Fig. 1. (a) ICP analyses of $PW_{15}V_3$@MIL-101 with different loadings of the $PW_{15}V_3$. (b) TGA of MIL-101 and $PW_{15}V_3$@MIL-101 under N_2. (c) IR spectra of $PW_{15}V_3$, MIL-101, as-synthesized $PW_{15}V_3$@MIL-101 and $PW_{15}V_3$@MIL-101 after photocatalytic reactions. (d) XRD patterns of MIL-101 and $PW_{15}V_3$@MIL-101: the calculated XRD pattern of MIL-101, the as-synthesized MIL-101, and $PW_{15}V_3$@MIL-101 before and after the photocatalytic reaction.

POM@5MOFs for V-1 to V-7, respectively. In the formula, the $\{\alpha\text{-}P_2W_{15}V_3O_{62}\}^{9-}$ (α-$PW_{15}V_3$) anion with 9 negative charges was used to decorate the MOF $[Cr_3O(H_2O)_2(OH)(O_2C{-}C_6H_4{-}CO_2)_3]$, which shows the dynamic surface charge status of the POM@MOF versus the amount of POMs. TG analysis of the samples as prepared is shown in Fig. 1b and S3, with $P_2W_{15}V_3$@MIL-101 exhibiting a lower weight loss than that of the isolated MIL-101. The difference in weight loss confirms the combination of the POM and the framework. In Fig. 1c, the vibrational bands of MIL-101 around 1670, 1613, 1551, 1433, 1400 cm^{-1}, and the peaks of the $PW_{15}V_3$ located at 1075, 1045, 1010, 935, 875, 765 cm^{-1} were all observed in the IR spectrum of the $PW_{15}V_3$@MIL-101 (Fig. S2). The XRD patterns of MIL-101 and $PW_{15}V_3$@MIL-101 are very similar to the calculated pattern (Fig. 1d), revealing that the crystalline composite of the isolated MOF possessed the framework structure of MIL-101, which was retained after loading the POMs. Additionally, EDX (Fig. S1a) and high-resolution scanning electron microscope (HSEM) and corresponding elemental mapping analysis (Fig. S4) of the composites indicate that the elements C, O, Cr and W all homogeneously distribute and overlap on the nanoparticles. These results together with the TG, IR, ICP and sorption isotherms could confirm the successful combination of POMs with the porous MIL-101 framework (Fig. S5).

To evaluate the ability of these composites to absorb dyes of different charges, we chose cationic methylene blue (MB) and anionic methyl orange (MO) for use as model molecules in the absorption experiments. MIL-101 (15 mg) and **V-6** (15 mg) were each added into 100 mL dye solution. Then, the UV–vis absorption spectra of these dye solutions were tested. As shown in Fig. 2a and b, when MIL-101 was added into the MO solution, the absorption peak (at 460 nm) disappeared more quickly than that of **V-6** in the same solution. The adsorption ratio of MIL-101 was 67%, and that of **V-6** was 11%. In this MIL-101 framework, no fluorine and chlorine are present. The anionic dyes could be encapsulated inside the mesoporous cavities of MIL-101. However, it is incompatible with cationic dyes. In the POM@MOF material, the polyanions are also hosted in the MOF governed by ionic interactions between anionic POM and cationic MOF $\{Cr_3O(H_2O)_{2+x}(OH)_{1-x}[(CO_2)\text{-}C_6H_3\text{-}(CO_2)_3]_3\}$ [61,62]. PSs for photocatalytic water-splitting are usually cationic dye molecules. Here, polyoxoaions with highly negative charges were introduced into MIL-101 to compensate its charge. When **V-6** was added into 100 mL MB solution, the peak of MB (at 660 nm) declined more quickly than that of MIL-101 (15 mg). The adsorption efficiency of **V-6** towards MB was about 99%, much higher than that of MIL-101 (Fig. 2c, d). We performed the adsorption experiment of **V-6** in the mixed solution of MO and MB (10 mg L^{-1} MO and 10 mg L^{-1} MB) under similar conditions. The MB was almost adsorbed completely; in contrast, trace MO was removed from the mixed solution (Fig. 2e, f). The above experiments showed that the charge of MIL-101 was over-compensated via the introduction of the negatively charged polyoxoanion. These POM@MOF composites can thus accommodate cationic dye molecules.

Ru – polypyridyl chromophores have been considered effective cationic PSs because they can be readily excited by visible light to an excited state. We believe these cationic PSs could be encapsulated by anionic molecular porous materials, resulting in photoactive composites. To evaluate their adsorption activity, we measured UV–vis absorption spectra of $[Ru(bpy)_3]^{2+}$ solution in the presence of MIL-101 and POM@MIL-101. As shown in Fig. 3a, the absorbance of cationic PS remained almost unchanged over time in the presence of the MIL-101 framework, indicating that MIL-101 could not absorb the cationic PS. For **V-1** and **V-6**, *ca.* 50% or 70% $[Ru(bpy)_3]^{2+}$ was encapsulated in the anionic POM@MOF frameworks, illustrating that anionic $PW_{15}V_3$@MIL-101 can absorb more of the cationic PS $[Ru(bpy)_3]^{2+}$ than MIL-101. Furthermore, the absorption ability of the POM@MOF was greatly enhanced by increasing the loading amount of the polyoxoanion (Fig. 3b and S6). These results confirmed the efficiency of our strategy for adjusting the ability of the MOFs to absorb anionic and cationic molecules. We thus present a simple strategy for constructing a photosensitizing composite by combining cationic PSs with catalyst-containing MOF frameworks.

The $[Ru(bpy)_3]^{2+}$ can be readily excited by visible light to a ^{1}MLCT excited state. It can then efficiently transfer to the ^{3}MLCT state through intersystem crossing. A facile electron transfer process from excited states to the electron acceptor usually occurs in the photocatalytic process. To assess the electron transfer process of our photocatalytic reaction system, the luminescence spectroscopy of the PS $Ru(bpy)_3^{2+}$ in

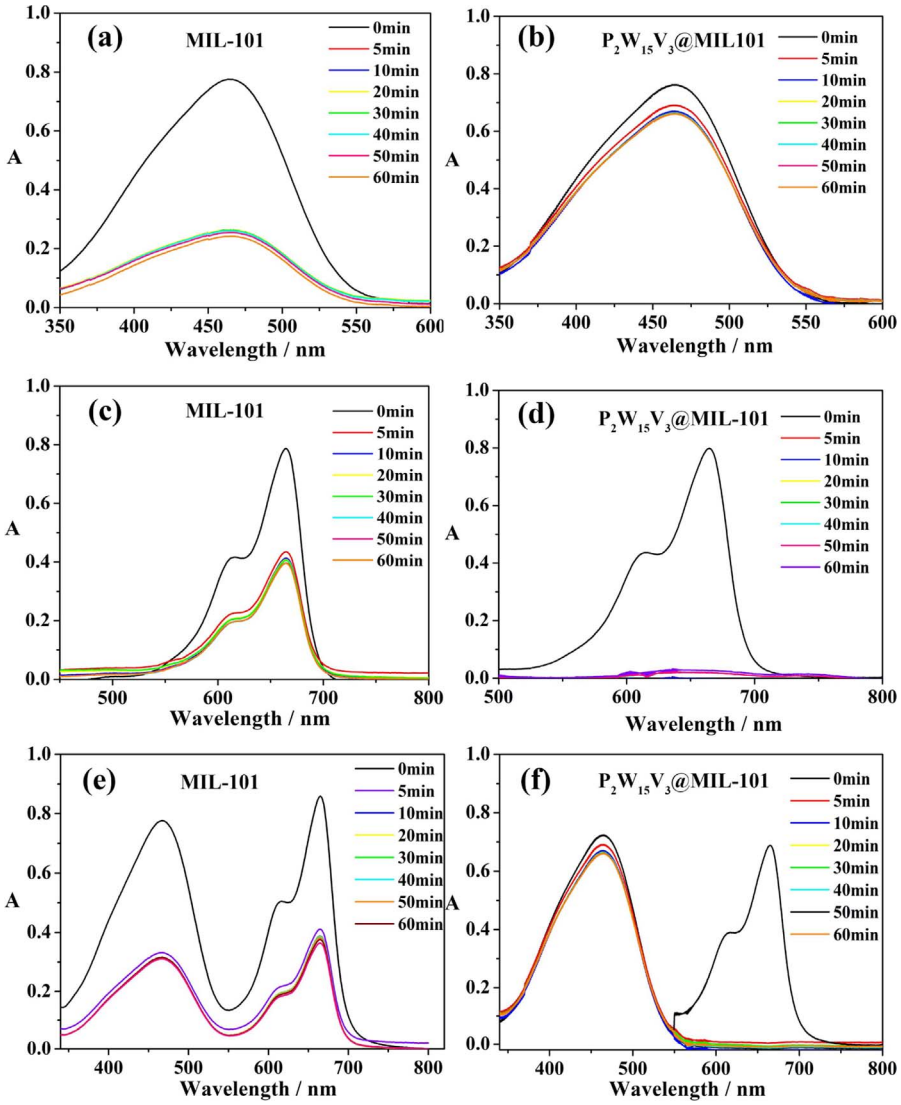

Fig. 2. UV–vis spectra of the dye solution containing MIL-101 and **V-6**: (a, b) 10 mg L^{-1} MO; (c, d) 10 mg L^{-1} MB; (e, f) mixed solution of 10 mg L^{-1} MO and MB.

CH_3CN/DMF (3/7) was measured as a function of the concentrations of TEOA, $P_2W_{15}V_3$, $P_2W_{17}Ni$, and $P_2W_{17}Co$. Steady-state photoluminescence spectroscopy shows that the ^{3}MLCT state of $[Ru(bpy)_3]^{2+}$ emissions were reduced when the concentration of TEOA or POMs was increased (Fig. 4a, S7). Time-resolved fluorescence spectroscopy confirms that $P_2W_{15}V_3$ can accelerate the luminescence decay of the ^{3}MLCT of $Ru(bpy)_3^{2+}$ with a lifetime from 178 ns to 148 ns. $P_2W_{17}Ni$, $P_2W_{17}Co$ can also accelerate the luminescence decay of $Ru(bpy)_3^{2+}$* (161 ns and 172 ns, respectively) (Fig. 4b–d). These results indicated facile electron transfer from the excited states of $Ru(bpy)_3^{2+}$ to the POMs, suggesting that POMs could be used for visible light-driven proton reduction. Further, MIL-101-Al and MIL-101-Fe were also synthesized, which possess of similar PXRD pattern with that of MIL-101-Cr (Fig. S8). These isolated frameworks all only absorb trace amount of the cationic PS $[Ru(bpy)_3]^{2+}$. Steady-state photoluminescence spectroscopy (Fig. S9) and transient fluorescence spectroscopy (Fig. S10) proved that these isolated platforms of MIL-101 can not assess the electron transfer process of the photocatalytic reaction system.

Photocatalytic hydrogen production of the POM@MIL-101 assembly was performed under visible-light irradiation by 300 W Xe light (> 420 nm). In a typical experiment, the POM@MIL-101 composite was added to the DMF/CH_3CN (7/3) mixed solution in the presence of 200 μL H_2O, with TEOA as the sacrificial electron donor. The amount of H_2 produced was quantified by gas chromatography. The H_2 evolved under visible light irradiation at a rate of 883 μmol h^{-1} g^{-1} in 8 h with respect to $[P_2W_{15}V_3O_{62}]^{6-}$. After a 8 h irradiation, the turnover numbers (TON) of **V-1** reached 56 ([defined as n(1/2H_2)/n(POM)]). As shown in Fig. 3, the amount of H_2 production was greatly improved by encapsulating $P_2W_{15}V_3$ in MIL-101 cages. Furthermore, two other POMs, $P_2W_{17}Ni$ and $P_2W_{17}Co$, were encapsulated in the cages of MIL-101 by a similar method and used for photocatalytic H_2 production (Fig. S11–S13). After a 8 h visible-light irradiation under similar conditions, the TONs of **Ni-1** and **Co-1** are 50 and 49, respectively. The photocatalytic performances of $P_2W_{17}Ni$@MIL-101 and $P_2W_{17}Co$@MIL-101 are all much higher than that of the homogeneous photocatalytic system. The chemical environmental control of the MOF molecular platform can enrich cationic PS $[Ru(bpy)_3]^{2+}$ in the solution, allowing it to surround and make effective contact with the catalysts, resulting in far higher photocatalytic activity than that of the homogeneous catalytic system. We performed control experiments in the absence of catalysis (POM@MIL-101), H_2O, or TEOA under the same conditions. The isolated MIL-101 was used as the catalyst in our study of the photocatalytic reaction, only a trace amount of H_2 production could be detected after a 8 h irradiation (Fig. S11).

The stability and recyclability of $PW_{15}V_3$@MIL-101 are demonstrated in photocatalytic H_2 production. After each cycle, the adsorbent $[Ru(bpy)_3]^{2+}$ was separated by centrifugation and ultrasonically washed several times at room temperature with a dilute solution of NaCl,

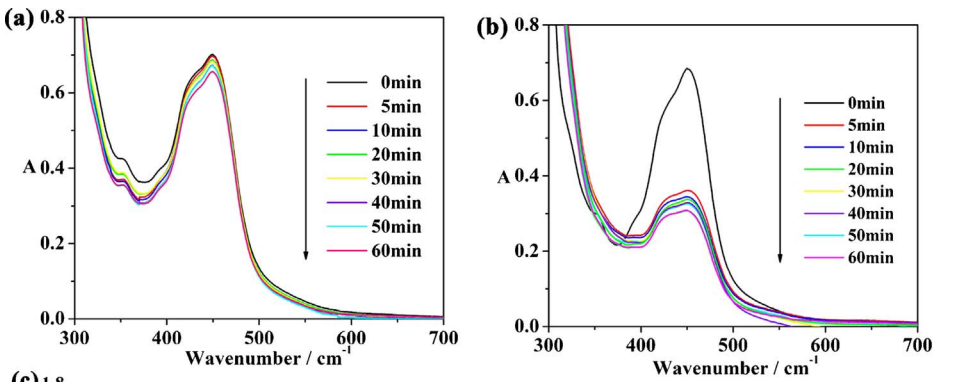

Fig. 3. UV–vis spectra of $[Ru(bpy)_3]^{2+}$ (48 μM) solution in the presence of 10 mg (a) isolated MIL-101 and (b) **V-1**. (c) Kinetics of H_2 production in the photocatalytic system with different catalysts. (d) Kinetics of H_2 production in the photocatalytic system with Mo_2S_{12}.

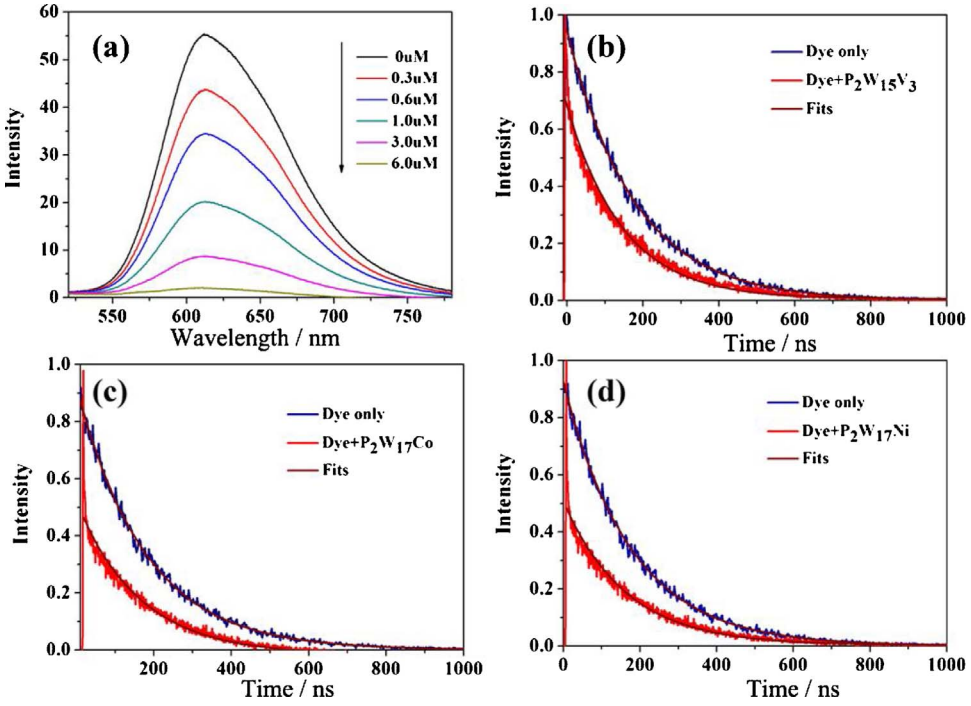

Fig. 4. (a) Steady-state photoluminescence spectroscopy of $Ru(bpy)_3^{2+}$ (48 μM) as a function of $P_2W_{15}V_3$ concentration; (b, c, d) Transient fluorescence spectroscopy measured at 620 nm (λ_{ex} = 485 nm) of $Ru(bpy)_3^{2+}$ (48 μM) with 3.1 μM $P_2W_{15}V_3$, $P_2W_{17}Co$ and $P_2W_{17}Ni$, respectively.

DMF, and CH_3OH. Then, the regenerated $PW_{15}V_3$@MIL-101 was added to the same catalytic system. As shown in Fig. S12, the catalytic activity of POM@MIL-101 remained nearly unchanged after three cycles. The XRD patterns of POM@MIL-101 after photocatalytic reactions are similar to those of the as-synthesized sample (Fig. 1d), indicating that the molecular composite kept its structural integrity during the photocatalytic reaction.

The above results confirm that the MOF platform enriches PS molecules and enhances the photocatalytic efficiency of the POMs. The enrichment process of the POMs was achieved in the synthesis of the composite POM@MOF, which also enhanced the photocatalytic efficiency. The successful introduction of different POMs suggests the universality of our method. To confirm this hypothesis, we selected a smaller metal-S cluster $[Mo_2(S_2)_6]^{2-}$ (Mo_2S_{12}) with excellent electrocatalytic activity for hydrogen production that could enter into MOFs freely.[59] MIL-101 was soaked in DMF solution containing anionic Mo_2S_{12} for 12 h. The Mo_2S_{12} cluster was successfully loaded and enriched into the MIL-101, resulting in a Mo_2S_{12}@MIL-101 composite, which we confirmed by ICP. Under the same conditions, the H_2 evolved at a rate of 25578 μmol h^{-1} g^{-1} after a 8 h irradiation in the DMF solution, much higher than that of the homogeneous system (Fig. 3d). The H_2 production in the photocatalytic system with different platform Mo_2S_{12}@MIL-101(Cr), Mo_2S_{12}@MIL-101(Fe) and Mo_2S_{12}@MIL-101(Al) shows that excellent hydrogen production activity with an

evolution rate of 25578 μmol $h^{-1}g^{-1}$, 21732 μmol $h^{-1}g^{-1}$ and 27082 μmol $h^{-1}g^{-1}$ respectively after a 8 h irradiation, higher than that of the homogeneous system (Fig. S13).

4. Conclusions

We have developed a simple, efficient and universal method for constructing photocatalytic active MOF-based composite materials by immobilizing polyoxoanions into porous framework materials. This greatly improves their ability to adsorb cationic PSs. The introduction of POMs into the MOF framework not only causes the polyoxoanions to arrange themselves uniformly in the 3D matrix, but also enriches the PSs, allowing them to surround around and make effective contact with catalysts. We successfully introduced three polyoxoanions $P_2W_{15}V_3$, $P_2W_{17}Ni$ and $P_2W_{17}Co$ into the MIL-101 framework, resulting in anionic POM@MOF composites. The POM@MIL-101 composites exhibited different catalytic activity with different POMs: the catalytic performance of $P_2W_{15}V_3$@MIL-101 was higher than that of the $P_2W_{17}Ni$@MIL-101 and $P_2W_{17}Co$@MIL-101 composites, which were similar to the trend of homogeneous systems. Their photocatalytic activity was greater than that of the homogeneous catalytic system. We selected a smaller metal-sulfur cluster Mo_2S_{12} that could enter the MOFs freely to use as the anionic unit and catalytic center. The hydrogen production rate can reach up to 25578 μmol $h^{-1}g^{-1}$ by enriching both the anionic Mo_2S_{12} clusters and cationic PSs in the porous MOF platform. Further studies will focus on finding and introducing more efficient molecular cluster catalysts into the MOF platform to create useful molecular devices.

Acknowledgments

This work was supported by the National Natural Science Foundation of China (No. 21671032/21722104), Natural Science Foundation of Tianjin City (17JCQNJC05100), Science and Technology Development Project Foundation of Jilin Province (20150520001JH), Science and Technology Research Foundation of the Thirteenth Five Years of Jilin Educational Committee ([2015]0056/JJKH20170605KJ).

Appendix A. Supplementary data

Supplementary data associated with this article can be found, in the online version, at http://dx.doi.org/10.1016/j.apcatb.2017.10.031.

References

[1] T. Zhang, W. Lin, Metal-organic frameworks for artificial photosynthesis and photocatalysis, Chem. Soc. Rev. 43 (2014) 5982–5993.
[2] L.Q. Jing, W. Zhou, G.H. Tian, H.G. Fu, Surface tuning for oxide-based nanomaterials as efficient photocatalysts, Chem. Soc. Rev. 42 (2013) 9509–9549.
[3] X. Zong, H. Yan, G. Wu, G. Ma, F. Wen, L. Wang, C. Li, Enhancement of photocatalytic H_2 evolution on CdS by loading MoS_2 as cocatalyst under visible light irradiation, J. Am. Chem. Soc. 130 (2008) 7176–7177.
[4] H.L. Wang, L.S. Zhang, Z.G. Chen, J.Q. Hu, S.J. Li, Z.H. Wang, J.S. Liu, X.C. Wang, Semiconductor heterojunction photocatalysts: design, construction, and photocatalytic performances, Chem. Soc. Rev. 43 (2014) 5234–5244.
[5] Y. Wang, F. Li, X. Zhou, F. Yu, J. Du, L. Bai, L. Sun, Highly efficient photoelectrochemical water splitting with an immobilized molecular Co_4O_4 cubane catalyst, Angew. Chem. Int. Ed. 56 (2017) 6911–6915.
[6] V. Singh, Z. Chen, P. Ma, D. Zhang, M.G.B. Drew, J. Niu, J. Wang, Unprecedented $\{Fe_{14}\}/\{Fe_{10}\}$ polyoxotungstate-based nanoclusters with efficient photocatalytic H_2 evolution activity: synthesis, structure, magnetism, and electrochemistry, Chem. Eur. J. 22 (2016) 10983–10989.
[7] D.Y. Shi, C. He, B. Qi, C. Chen, J.Y. Niu, C.Y. Duan, Merging of the photocatalysis and copper catalysis in metal-organic frameworks for oxidative C–C bond formation, Chem. Sci. 6 (2015) 1035–1042.
[8] V. Duros, J. Grizou, W. Xuan, Z. Hosni, D.-L. Long, H.N. Miras, L. Cronin, Mixed-valence manganese cubane trapped by inequivalent trilacunary polyoxometalate ligands, Angew. Chem. Int. Ed. 56 (2017), http://dx.doi.org/10.1002/anie.201705721.
[9] H.J. Lv, Y.V. Geletii, C.C. Zhao, J.W. Vickers, G.B. Zhu, Z. Luo, J. Song, T.Q. Lian, D.G. Musaev, C.L. Hill, Polyoxometalate water oxidation catalysts and the production of green fuel, Chem. Soc. Rev. 41 (2012) 7572–7589.
[10] Z.-J. Liu, X.-L. Wang, C. Qin, Z.-M. Zhang, Y.-G. Li, W.-L. Chen, E.-B. Wang, Coord. Polyoxometalate-assisted synthesis of transition-metal cubane clusters as artificial mimics of the oxygen-evolving center of photosystem II, Chem. Rev. 313 (2016) 94–110.
[11] X.-B. Han, Z.-M. Zhang, T. Zhang, Y.-G. Li, W. Lin, W.-S. You, Z.-M. Su, E.-B. Wang, Polyoxometalate-based cobalt–phosphate molecular catalysts for visible light-driven water oxidation, J. Am. Chem. Soc. 136 (2014) 5359–5366.
[12] J. Dong, J. Hu, Y. Chi, Z. Lin, B. Zou, S. Yang, C.L. Hill, C. Hu, A polyoxoniobate–polyoxovanadate double-anion catalyst for simultaneous oxidative and hydrolytic decontamination of chemical warfare agent simulants, Angew. Chem. Int. Ed. 56 (2017) 4473–4477.
[13] P. Argitis, E.J. Papaconstantinou, Photoch Photocatalytic multielectron photoreduction of 18-tungstodiphosphate in the presence of organic compounds — production of hydrogen, J. Photochem. 30 (1985) 445–451.
[14] S.J. Li, S.M. Liu, S.X. Liu, Y.W. Liu, Q. Tang, Z. Shi, S.X. Ouyang, J.H. Ye, $\{Ta_{12}\}/\{Ta_{16}\}$ cluster-containing polytantalotungstates with remarkable photocatalytic H_2 evolution activity, J. Am. Chem. Soc. 134 (2012) 19716–19721.
[15] H.-L. Wu, Z.-M. Zhang, Y.-G. Li, X.-L. Wang, E.-B. Wang, Recent progress in polyoxoniobates decorated and stabilized via transition metal cations or clusters, Cryst. Eng. Comm. 17 (2015) 6261–6268.
[16] X.Q. Du, J. Zhao, J. Mi, Y. Ding, P. Zhou, B. Ma, J. Zhao, J. Song, Efficient photocatalytic H_2 evolution catalyzed by an unprecedented robust molecular semiconductor $\{Fe_{11}\}$ nanocluster without cocatalysts at neutral conditions, Nano Energy 16 (2015) 247–255.
[17] F.Y. Song, Y. Ding, B.C. Ma, C.G. Wang, Q. Wang, X.Q. Du, S. Fu, J. Song, Engineering of ZnCo-layered double hydroxide nanowalls toward high-efficiency electrochemical water oxidation, Energy Environ. Sci. 6 (2013) 1170–1184.
[18] H.J. Lv, W.W. Guo, K.F. Wu, Z.Y. Chen, J. Bacsa, D.G. Musaev, Y.V. Geletii, S.M. Lauinger, T.Q. Lian, A noble-metal-free, tetra-nickel polyoxotungstate catalyst for efficient photocatalytic hydrogen evolution, J. Am. Chem. Soc. 136 (2014) 14015–14018.
[19] W.M. Wu, T. Teng, X.Y. Wu, X.Z. Dui, L. Zhang, J.H. Xiong, L. Wu, C.Z. Lu, A cobalt-based polyoxometalate catalyst for efficient visible-light-driven H_2 evolution from water splitting, Catal. Commun. 64 (2015) 44–47.
[20] M. Murakami, D. Hong, T. Suenobu, S. Yamaguchi, T. Ogura, S.J. Fukuzumi, Catalytic mechanism of water oxidation with single-site ruthenium-heteropolytungstate complexes, J. Am. Chem. Soc. 133 (2011) 11605–11613.
[21] J.-Q. Shen, Y. Zhang, Z.-M. Zhang, Y.-G. Li, Y.-Q. Gao, E.-B. Wang, Polyoxoniobate-based 3D framework materials with photocatalytic hydrogen evolution activity, Chem. Commun. 50 (2014) 6017–6019.
[22] J.H. Son, J. Wang, F.E. Osterloh, P. Yu, W.H. Casey, A tellurium-substituted Lindqvist-type polyoxoniobate showing high H_2 evolution catalyzed by tellurium nanowires via photodecomposition, Chem. Commun. 50 (2014) 836–838.
[23] H.C. Zhou, J.R. Long, O.M. Yaghi, Introduction to metal-organic frameworks, Chem. Rev. 112 (2012) 673–674.
[24] Y. Liu, W.M. Xuan, Y. Cui, Engineering homochiral metal-organic frameworks for heterogeneous asymmetric catalysis and enantioselective separation, Adv. Mater. 22 (2010) 4112–4135.
[25] Q.L. Zhu, Q. Xu, Metal–organic framework composites, Chem. Soc. Rev. 43 (2014) 5468–5512.
[26] J.Y. Lee, O.K. Farha, J. Roberts, K.A. Scheidt, S.T. Nguyen, J.T. Hupp, Metal–organic framework materials as catalysts, Chem. Soc. Rev. 38 (2009) 1450–1459.
[27] J.W. Liu, L.F. Chen, H. Cui, J.Y. Zhang, L. Zhang, C.Y. Su, Applications of metal-organic frameworks in heterogeneous supramolecular catalysis, Chem. Soc. Rev. 43 (2014) 6011–6061.
[28] S. Pullen, H. Fei, A. Orthaber, S.M. Cohen, S. Ott, Enhanced photochemical hydrogen production by a molecular diiron catalyst incorporated into a metal-organic framework, J. Am. Chem. Soc. 135 (2013) 16997–17003.
[29] P.-Q. Liao, N.-Y. Huang, W.-X. Zhang, J.-P. Zhang, X.-M. Chen, Controlling guest conformation for efficient purification of butadiene, Science 356 (2017) 1193–1196.
[30] D.Y. Du, J.S. Qin, S.L. Li, Z.M. Su, Y.Q. Lan, Recent advances in porous polyoxometalate-based metal-organic framework materials, Chem. Soc. Rev. 43 (2014) 4615–4632.
[31] Q. Yang, Q. Xu, S.-H. Yu, H.-L. Jiang, Pd nanocubes@ZIF-8: integration of plasmon-driven photothermal conversion with a metal–organic framework for efficient and selective catalysis, Angew. Chem. Int. Ed. 55 (2016) 3685–3689.
[32] R. Li, X.Q. Ren, J.S. Zhao, X. Feng, X. Jiang, X.X. Fan, Z.G. Lin, X.G. Li, C.W. Hu, B. Wang, Polyoxometallates trapped in a zeolitic imidazolate framework leading to high uptake and selectivity of bioactive molecules, J. Mater. Chem. A. 2 (2014) 2168–2173.
[33] Y.N. Gong, T. Ouyang, C.T. Hea, T.B. Lu, Photoinduced water oxidation by an organic ligand incorporated into the framework of a stable metal–organic framework, Chem. Sci. 7 (2016) 1070–1075.
[34] S.T. Zheng, X. Zhao, S. Lau, A. Fuhr, P.Y. Feng, X.H. Bu, Entrapment of metal clusters in metal–organic framework channels by extended hooks anchored at open metal sites, J. Am. Chem. Soc. 135 (2013) 10270–10273.
[35] (a) S. Zhao, Y. Wang, J. Dong, C.-T. He, H. Yin, P. An, K. Zhao, X. Zhang, C. Gao, L. Zhang, J. Lv, J. Wang, J. Zhang, A.M. Khattak, N.A. Khan, Z. Wei, J. Zhang, S. Liu, H. Zhao, Z. Tang, Ultrathin metal–organic framework nanosheets for electrocatalytic oxygen evolution, Nat. Energy 1 (2016) 1–10;
(b) J. Qin, D.-Y. Du, W. Guan, X.-J. Bo, Y.-F. Li, L.-P. Guo, Z.-M. Su, Y.-Y. Wang, Y.-Q. Lan, H.-C. Zhou, Ultrastable polymolybdate-based metal–organic frameworks as highly active electrocatalysts for hydrogen generation from water, J. Am. Chem. Soc. 137 (2015) 7169–7177.

[36] Q. Gao, J. Xu, D. Cao, Z. Chang, X.-H. Bu, A rigid nested metal–organic framework featuring a thermoresponsive gating effect dominated by counter ions, Angew. Chem. Int. Ed 55 (2016) 15027–15030.
[37] C.-Y. Sun, S.-X. Liu, D.-D. Liang, K.-Z. Shao, Y.-H. Ren, Z.-M. Su, Highly stable crystalline catalysts based on a microporous metal-organic framework and polyoxometalates, J. Am. Chem. Soc. 131 (2009) 1883–1888.
[38] H.-C. Hu, H.-S. Hu, B. Zhao, P. Cui, P. Cheng, J. Li, Metal–organic frameworks (MOFs) of a cubic metal cluster with multicentered Mn^{I} - Mn^{I} bonds, Angew. Chem. Int. Ed 54 (2015) 11681–11685.
[39] J.H. Cavka, S. Jakobsen, U. Olsbye, N. Guillou, C. Lamberti, S. Bordiga, K.P. Lillerud, A new zirconium inorganic building brick forming metal organic frameworks with exceptional stability, J. Am. Chem. Soc. 130 (2008) 13850–13851.
[40] G. Fére, C. Mellot-Draznieks, C. Serre, F. Millange, J. Dutour, S. Surblé, I. Margiolaki, A chromium terephthalate-based solid with unusually large pore volumes and surface area, Science 309 (2005) 2040–2042.
[41] J. Zheng, M.Y. Wu, F.L. Jiang, W.P. Su, M.C. Hong, Stable porphyrin Zr and Hf metal–organic frameworks featuring 2. 5 nm cages: high surface areas, SCSC transformations and catalyses, Chem Sci. 6 (2015) 3466–3470.
[42] Y. Inokuma, M. Kawano, M. Fujita, Crystalline molecular flasks, Nat. Chem. 3 (2011) 349–358.
[43] P. Serra-Crespo, E.V. Ramos-Fernandez, J. Gascon, Synthesis and characterization of an amino functionalized MIL-101(Al): separation and catalytic properties, Chem. Mater. 23 (2011) 2565–2572.
[44] K.M. Choi, K. Na, G.A. Somorjai, M.O. Yaghi, Chemical environment control and enhanced catalytic performance of platinum nanoparticles embedded in nanocrystalline metal–organic frameworks, J. Am. Chem. Soc. 137 (2015) 7810–7816.
[45] Y.X. Tan, Y. Zhang, Y.P. He, Y.J. Zheng, J. Zhang, Multifunctional anionic MOF material for dye enrichment and selective sorption of C_2 hydrocarbons over methane via Ag^{+}-exchange, Inorg. Chem. 53 (2014) 12973–12976.
[46] Y. Bai, Y. Dou, L. Xie, L.-H.W. Rutledge, J.-R. Li, H.-C. Zhou, Zr-based metal–organic frameworks: design, synthesis, structure, and applications, Chem. Soc. Rev. 45 (2016) 2327–2367.
[47] Z.-M. Zhang, T. Zhang, C. Wang, Z.-K. Lin, L.-S. Long, W.B. Lin, Photosensitizing metal–organic framework enabling visible-light-driven proton reduction by a Wells–Dawson-type polyoxometalate, J. Am. Chem. Soc. 137 (2015) 3197–3200.
[48] A.-X. Yan, S. Yao, Y.-G. Li, Z.-M. Zhang, Y. Lu, W.-L. Chen, E.-B. Wang, Incorporating polyoxometalates into a porous MOF greatly improves its selective adsorption of cationic dyes, Chem. Eur. J. 20 (2014) 6927–6933.
[49] X. Liu, W. Gong, J. Luo, C. Zou, Y. Yang, S. Yang, Selective adsorption of cationic dyes from aqueous solution bypolyoxometalate-based metal–organic framework composite, Appl. Surf. Sci. 362 (2016) 517–524.
[50] C. Zou, Z.J. Zhang, X. Xu, Q.H. Gong, J. Li, C.D. Wu, A multifunctional organic–inorganic hybrid structure based on Mn^{III}–porphyrin and polyoxometalate as a highly effective dye scavenger and heterogenous catalyst, J. Am. Chem. Soc. 134 (2012) 87–90.
[51] W.-Y. Gao, M. Chrzanowski, S. Ma, Metal–metalloporphyrin frameworks: a resurging class of functional materials, Chem. Soc. Rev. 43 (2014) 5841–5866.
[52] I. Hod, M.D. Sampson, P. Deria, C.P. Kubiak, O.K. Farha, J.T. Hupp, Fe-porphyrin-based metal–organic framework films as high-surface concentration, heterogeneous catalysts for electrochemical reduction of CO_2, ACS Cata. 5 (2015) 6302–6309.
[53] X.Y. Dong, M. Zhang, R.B. Pei, Q. Wang, D.H. Wei, S.Q. Zang, Y.T. Fan, T.C.W. Mak, A crystalline copper(II) coordination polymer for the efficient visible-light-driven generation of hydrogen, Angew. Chem. Int. Ed. 55 (2016) 2073–2077.
[54] R.W. Liang, R. Chen, F.F. Jing, N. Qin, L. Wu, Multifunctional polyoxometalates encapsulated in MIL-100(Fe): highly efficient photocatalysts for selective transformation under visible light, Dalton Trans. 44 (2015) 18227–18236.
[55] C. Wang, K.E. deKrafft, W. Lin, Pt nanoparticles@photoactive metal–organic frameworks: efficient hydrogen evolution via synergistic photoexcitation and electron injection, J. Am. Chem. Soc. 134 (2012) 7211–7214.
[56] C. Wang, Z. Xie, K.E. deKrafft, W. Lin, Doping metal–organic frameworks for water oxidation, carbon dioxide reduction, and organic photocatalysis, J. Am. Chem. Soc. 133 (2011) 13445–13454.
[57] X.-J. Kong, Z. Lin, Z.-M. Zhang, T. Zhang, W. Lin, Hierarchical integration of photosensitizing metal–organic frameworks and nickel-containing polyoxometalates for efficient visible-light-driven hydrogen evolution, Angew. Chem. Int. Ed. 55 (2016) 6411–6416.
[58] R.G. Finke, B. Rapko, R.J. Saxton, J.D. Peter, Trisubstituted heteropolytungstates as soluble metal oxide analogues. 3.[1] synthesis characterization, ^{31}P, ^{29}Si, ^{51}V, and 1- and 2-D ^{183}W NMR, deprotonation, and H^{+} mobility studies of organic solvent soluble forms of $H_XSiW_9V_{30}O_{40}{}^{X-7}$ and $H_XP_2W_{15}V_3O_{62}{}^{X-9}$, J. Am. Chem. Soc. 108 (1986) 2947–2960.
[59] D.K. Lyon, W.K. Miller, T. Novet, P.J. Domaille, E. Evitt, D.C. Johnson, G.F. Richard, Highly oxidation resistant inorganic-porphyrin analogue polyoxometalate oxidation catalysts. 1. the synthesis and characterization of aqueous-soluble potassium salts of α_2-$P_2W_{17}O_{61}$ $(M^{n+}{\cdot}OH_2)^{(n?10)}$ and organic solvent soluble tetra-n-butylammonium salts of $_{\alpha 2}$-$P_2W_{17}O_{61}$ $(M^{n+}{\cdot}Br)^{(n?11)}$ (M = Mn^{3+}, Fe^{3+}, Co^{2+}, Ni^{2+}, Cu^{2+}), J. Am. Chem. Soc. 113 (1991) 7209–7221.
[60] Z.J. Huang, W.J. Luo, L. Ma, M.Z. Yu, X.D. Ren, M.F. He, S. Polen, K. Click, B.J. Garrett, J. Lu, K. Amine, C. Hadad, W.L. Chen, A. Asthagiri, Y.Y. Wu, Dimeric $[Mo_2S_{12}]^{2-}$ cluster: a molecular analogue of MoS_2 edges for superior hydrogen-evolution electrocatalysis, Angew. Chem. Int. Ed. 54 (2015) 15181–15185.
[61] R. Canioni, C. Roch-Marchal, F. Sécheresse, P. Horcajada, C. Serre, M. Hardi-Dan, G. Férey, J.-M. Grenèche, F. Lefebvre, J.-S. Chang, Y.-K. Hwang, O. Lebedev, S. Turnerf, G.V. Tendeloo, Stable polyoxometalate insertion within the mesoporous metal organic framework MIL-100(Fe), J. Mater. Chem. 21 (2011) 1226–1233.
[62] J.-W. Sun, P.-F. Yan, G.-H. An, J.-Q. Sha, G.-M. Li, G.-Y. Yang, Immobilization of polyoxometalate in the metal-organic framework rht-MOF-1: towards a highly effective heterogeneous catalyst and dye scavenger, Sci. Rep. 6 (2016) 25595.